

Transport between edge states in multilayer integer quantum Hall systems: exact treatment of Coulomb interactions and disorder

J. W. Tomlinson,¹ J.-S. Caux,² and J. T. Chalker¹

¹*Theoretical Physics, University of Oxford, 1 Keble Road, OX1 3NP, United Kingdom.*

²*Institute for Theoretical Physics, University of Amsterdam, Valckenierstraat 65, 1018 XE Amsterdam, The Netherlands.*

(Dated: November 7, 2018)

A set of stacked two-dimensional electron systems in a perpendicular magnetic field exhibits a three-dimensional version of the quantum Hall effect if interlayer tunneling is not too strong. When such a sample is in a quantum Hall plateau, the edge states of each layer combine to form a chiral metal at the sample surface. We study the interplay of interactions and disorder in transport properties of the chiral metal, in the regime of weak interlayer tunneling. Our starting point is a system without interlayer tunneling, in which the only excitations are harmonic collective modes: surface magnetoplasmons. Using bosonization and working perturbatively in the interlayer tunneling amplitude, we express transport properties in terms of the spectrum for these collective modes, treating electron-electron interactions and impurity scattering exactly. We calculate the conductivity as a function of temperature, finding that it increases with increasing temperature as observed in recent experiments. We also calculate the autocorrelation function of mesoscopic conductance fluctuations induced by changes in a magnetic field component perpendicular to the sample surface, and its dependence on temperature. We show that conductance fluctuations are characterised by a dephasing length that varies inversely with temperature.

PACS numbers: 73.20.-r, 73.23.-b, 72.20.-i, 73.21.Ac

I. INTRODUCTION

Multilayer quantum Hall systems offer a setting in which to study the influence of electron-electron interactions and impurity scattering on tunneling between quantum Hall edge states. Specifically, consider a layered conductor in a magnetic field that is perpendicular to the layers, with the field strength chosen so that a single layer in isolation would have quantised Hall conductance. Then, if interlayer tunneling is not too strong, the multilayer system exhibits a three-dimensional version of the quantum Hall effect and the bulk is insulating at low temperatures. Under these conditions, edge states are present in each layer at the sample surface and are coupled by interlayer tunneling to form a surface phase, which is a chiral, two-dimensional metal.^{1,2} The contribution of this surface phase to the interlayer electron transport properties of such systems has been isolated in experiments on semiconductor multilayers,³ and is dominant if samples are sufficiently small and cold.

The consequences of impurity scattering for transport in the chiral metal have been discussed extensively from a theoretical viewpoint^{1,2,4,5,6,7,8,9} and have been probed experimentally in several ways.^{3,10,11,12,13,14,15,16,17,18,19} Crucially, the chiral motion of electrons along the layer edges means that localisation is suppressed.^{1,2} As a result, the surface conductivity in the interlayer direction has a low-temperature limit that is non-zero, even though its measured value may be much smaller than e^2/h .^{3,11,13} Separately, theoretical discussions of conductance fluctuations^{4,5,6,7,9} have examined both their dependence on geometry in fully phase-coherent samples, and their dependence on the inelastic scattering length when

this is smaller than sample size. Observations of reproducible mesoscopic conductance fluctuations,^{12,19} induced by small changes of magnetic field within a quantum Hall plateau, demonstrate that interlayer hopping is quantum-mechanically coherent and also provide a way to determine the inelastic scattering length. In addition, magnetoresistance in response to a field component perpendicular to the sample surface has been proposed⁸ and used^{14,15,17} as a method for measuring the elastic scattering length.

In contrast to these studies of disorder effects, past theoretical work on effects due to electron-electron interactions in the chiral metal has been limited. There have been discussions, first, of the temperature dependence of the inelastic scattering length^{2,9} and, second, of the fact that there is no zero-bias anomaly in the tunneling density of states (or any related contribution to the conductivity), because of ballistic motion of charge in the in-layer direction.^{2,9}

Against this background, recent experiments finding a significant temperature dependence to the surface conductivity^{16,18} are striking as likely indications of interaction effects, and provide one of the motivations for the work we present here. In particular, the fact that conductivity is observed to *increase* with increasing temperature presents a puzzle for theory. Some straightforward potential explanations are specifically excluded by the experimental design: large ratios of sample perimeter to cross-sectional area ensure that surface states make the dominant contribution to the measured conductance; and sample perimeters much longer than the inelastic scattering length ensure that weak localisation effects are absent. For samples studied in Ref. 18, the measured

conductivity $\sigma(T)$ increases by about 7% in the temperature range from 50mK to 300mK, implying a temperature scale of $\sigma(T) \cdot [d\sigma(T)/dT]^{-1} \sim 4\text{K}$, which is similar to that for other interaction effects in quantum Hall systems

In this paper we study interactions and disorder in the chiral metal, working in the experimentally-relevant limit of weak interlayer tunneling. Treating tunneling perturbatively, Coulomb interactions and impurity scattering can be handled exactly by means of a straightforward application of bosonization. We calculate the full temperature dependence of the conductivity. We also study conductance fluctuations induced by magnetic field changes, obtaining their autocorrelation function and its dependence on temperature. Making appropriate parameter choices, our results for both quantities are consistent with experimental findings. A short account of this work has been presented previously, in Ref. 20.

Our work differs from most of the extensive literature on tunneling between quantum Hall edge states in two important ways. First, while much previous work has been concerned with edge states of fractional quantum Hall systems,^{21,22,23,24} including multilayer samples,^{25,26} our focus is on the integer quantum Hall effect. Second, whereas most past work (with some exceptions: see Refs. 27,28,29,30) has been restricted to systems with only short-range interactions, we find that the long-range nature of Coulomb interactions, which we treat in full, is central for the results we obtain.

The remainder of this paper is organised as follows. We develop a model for the chiral metal in Sec. II and show how bosonization can be used to give an exact description of the collective excitations. Sec. III contains calculations of the temperature dependence of the conductivity. We study conductance fluctuations in Sec. IV, and discuss our results in Sec. V.

II. MODELLING THE CHIRAL METAL

In this section we summarise the physical ingredients that are important for modelling transport between edge states in multilayer conductors and set out the lengthscales that characterise the system. We introduce a Hamiltonian in terms of fermionic operators for edge electrons. We bosonize this Hamiltonian, obtaining a result which is quadratic in boson operators if interlayer tunneling is omitted. Finally, we express the two-electron correlation function that is central to transport calculations in terms of boson correlators.

A. Ingredients, lengthscales, and parameters

A multilayer conductor is illustrated in Fig 1. We use coordinates with the x -axis parallel to the layer edges, and treat a sample of N layers with layer index n and layer spacing a . Consider the system in the presence of

a perpendicular magnetic field of strength B , with the chemical potential lying between the lowest and first excited Landau levels. In the bulk of the sample single particle states at energies close to the chemical potential are localised by disorder. At the sample surface in this energy range, edge states propagate in the confining potential $V_{\text{edge}}(y)$ at a velocity v . Interactions modify the confining potential and the edge velocity: we denote by v_F the velocity allowing for Hartree contributions. Edge states have a width w in the y -direction, which is set by the magnetic length l_B in a clean sample, and by the bulk localisation length ξ in the presence of impurities. We use a one-dimensional description of the edge state in each layer, projected onto the x -coordinate in the standard way.

Our theoretical treatment takes account only of one edge state in each layer and is therefore appropriate for a system in which electrons are spin polarised. In fact, some of the experiments we refer to, including those on the temperature-dependence of conductivity,¹⁸ are for systems with Landau level filling factor per layer of $\nu = 2$. It is appropriate to apply our theory to these systems provided electrons with opposite spin directions contribute additively and incoherently to the conductivity.

The system of edge states can be characterised using three lengthscales. First, impurities, which generate only forward scattering with a phase shift, result in an elastic mean free path l_{el} , the distance over which a phase shift of order 2π is accumulated. Second, temperature T in combination with the velocity v_F can be expressed in terms of the thermal length $L_T = \hbar v_F / k_B T$. Third, interlayer tunneling with amplitude t_{\perp} can be parameterised by the characteristic distance l_{\perp} through which electrons move in the chiral direction between tunneling events. The value of l_{\perp} can be expressed in terms of the interlayer diffusion constant D : since, for small t_{\perp} , interlayer hops are of length a and occur at a rate v_F / l_{\perp} , one has $l_{\perp} = a^2 v_F / D$. In turn, this can be expressed in terms of the conductivity, using the Einstein relation and the fact that the density of states is $n = 1/2\pi a \hbar v_F$, giving $l_{\perp} = a(e^2/2\pi \hbar \sigma)$.⁹

Parameter values for the experiments of Refs. 3, 17 and 18 are as follows. Samples consist of $N \sim 50 - 100$ layers with spacing $a = 30\text{nm}$. The mean free path is estimated¹⁷ to be $l_{\text{el}} \sim 30\text{nm}$. An upper bound on v_F , reached in samples with a steep confining potential is $v_F \sim \omega_C l_B$, where ω_C is the cyclotron frequency. It has the value $\omega_C l_B = 1.7 \times 10^5 \text{ms}^{-1}$ in GaAs at 6.75 T. With this value, $L_T \sim 10\mu\text{m}$ at $T = 100\text{mK}$. Finally, for a surface conductivity of $\sigma = 1.3 \times 10^{-3} e^2/2\pi \hbar$ (which lies within the observed range at $\nu = 2$), $l_{\perp} = 40\mu\text{m}$. We are therefore concerned with the regime $l_{\text{el}} \ll L_T \ll l_{\perp}$, and this motivates our approach, based on a perturbative treatment of tunneling.

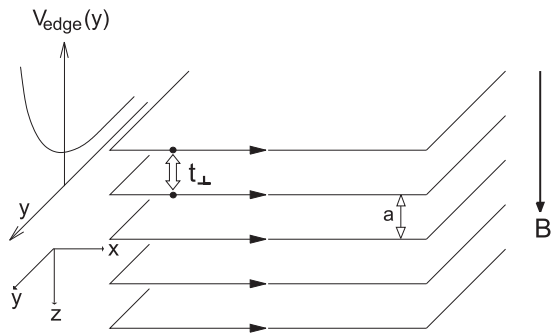


FIG. 1: A multilayer conductor, showing the orientation of axes in our coordinate system, with edge states propagating in the x -direction. The form of the confining potential $V_{\text{edge}}(y)$ is illustrated top left. Interlayer tunneling amplitude and spacing are denoted by t_{\perp} and a , respectively.

B. Fermionic Hamiltonian

Our model Hamiltonian, $\mathcal{H} = \mathcal{H}_0 + \mathcal{H}_{\text{dis}} + \mathcal{H}_{\text{hop}} + \mathcal{H}_{\text{int}}$, has single-particle terms \mathcal{H}_0 , \mathcal{H}_{dis} and \mathcal{H}_{hop} , representing, respectively, free motion along each edge, impurity scattering and interlayer hopping, and a contribution \mathcal{H}_{int} from Coulomb interactions. We write it in terms of the electron creation operator c_{qn}^{\dagger} for an edge state with wavevector q in layer n , taking sample perimeter L so that $q = 2\pi n_q/L$, where n_q is integer. The creation operator at a point is

$$\psi_n^{\dagger}(x) = \frac{1}{\sqrt{L}} \sum_{q=-\infty}^{\infty} e^{-iqx} c_{qn}^{\dagger}. \quad (2.1)$$

We normal order the Hamiltonian with respect to a vacuum in which states are occupied for $q \leq 0$ and empty otherwise. Then

$$\mathcal{H}_0 = -i\hbar v \sum_n \int dx : \psi_n^{\dagger}(x) \partial_x \psi_n(x) :, \quad (2.2)$$

and

$$\mathcal{H}_{\text{hop}} = \sum_n \int dx [t_{\perp} \psi_{n+1}^{\dagger}(x) \psi_n(x) + \text{H. c.}]. \quad (2.3)$$

The interaction contribution, written in terms of the projected density $\rho(x) = \psi_n^{\dagger}(x) \psi_n(x)$ with a two-particle potential $U_{n-m}(x-x')$, is

$$\mathcal{H}_{\text{int}} = \frac{1}{2} \sum_{nm} \int dx \int dx' : \rho_n(x) U_{n-m}(x-x') \rho_m(x') :. \quad (2.4)$$

Finally, writing the impurity potential projected onto the edge coordinate in the n th layer as $V_n(x)$, we have

$$\mathcal{H}_{\text{dis}} = \sum_n \int dx V_n(x) : \psi_n^{\dagger}(x) \psi_n(x) :. \quad (2.5)$$

We take $V_n(x)$ to be Gaussian distributed with zero-range correlations and strength Δ : $[V_n(x)]_{\text{av}} = 0$ and $[V_n(x)V_{n'}(x')]_{\text{av}} = \Delta \delta_{n,n'} \delta(x-x')$. This disorder term can be removed by means of a gauge transformation on the fermionic field operators, under which

$$\psi_n^{\dagger}(x) \rightarrow e^{i\theta_n(x)} \psi_n^{\dagger}(x), \quad (2.6)$$

where

$$\theta_n(x) = \frac{1}{\hbar v} \int_0^x dx' V_n(x') \quad (2.7)$$

is the phase shift acquired under forward scattering from the impurities. The elastic scattering length is related to the disorder strength Δ by $l_{\text{el}} = \hbar^2 v^2 / \Delta$. Under this gauge transformation, $\mathcal{H}_0 + \mathcal{H}_{\text{dis}} \rightarrow \mathcal{H}_0$. The hopping term, however, picks up a dependence on the disorder, and after the transformation is

$$\mathcal{H}_{\text{hop}} = \sum_n \int dx [t_{\perp}(n, x) \psi_{n+1}^{\dagger}(x) \psi_n(x) + \text{H. c.}], \quad (2.8)$$

where

$$t_{\perp}(n, x) = t_{\perp} e^{i(\theta_{n+1}(x) - \theta_n(x))}. \quad (2.9)$$

We ignore the effects of this gauge transformation on the boundary conditions applying to $\psi_n(x)$, which is justified at temperatures large compared to the single-particle level spacing. With this, $\mathcal{H}_0 + \mathcal{H}_{\text{int}}$ is unaffected by the gauge transformation, and gauge transformed operators c_{qn}^{\dagger} can be defined by inverting Eq. (2.1). All further references in this paper to fermionic operators are to the gauge-transformed ones.

C. Bosonised Hamiltonian

We bosonize the Hamiltonian in the standard way, expressing $\mathcal{H}_0 + \mathcal{H}_{\text{int}}$ in terms of non-interacting collective modes. Since \mathcal{H}_{hop} transforms into a cosine function of the boson creation and annihilation operators, we treat it perturbatively. To justify this, we require that t_{\perp} should be small. Since t_{\perp} is a relevant perturbation,²⁵ we also require that temperature should not be too small: $L_T \ll l_{\perp}$.

Boson creation operators are defined in the usual way (see, for example, Ref. 31) as

$$b_{qm}^{\dagger} = \frac{i}{(n_q)^{1/2}} \sum_{r=-\infty}^{\infty} c_{r+q,m}^{\dagger} c_{r,m} \quad (2.10)$$

for $q > 0$. Fourier transforming the interaction potential and expressing the result as a velocity, we introduce

$$u_{n-m}(q) = (2\pi\hbar)^{-1} \int dx e^{iqx} U_{n-m}(x). \quad (2.11)$$

The Fermi velocity renormalised by Hartree interactions is $v_F = v - \sum_n u_n(0)$, where the divergence which arises

in the sum in the case of Coulomb interactions is cancelled by contributions to v from a neutralising background. The Hamiltonian in the absence of hopping (and omitting fermion number terms which appear at electron densities different from that of our vacuum) is

$$\mathcal{H}_0 + \mathcal{H}_{\text{int}} = \sum_{mn} \sum_{q>0} \hbar[v_F + u_{n-m}(q)]qb_{qn}^\dagger b_{qm}. \quad (2.12)$$

The combination $\mathcal{H}_0 + \mathcal{H}_{\text{int}}$ is diagonalised by Fourier transform in the layer index n . We impose periodic boundary conditions on n , define the wavevector $k = 2n_k\pi/Na$, with n_k integer and $-\pi/a \leq k < \pi/a$, and set

$$b_{qk}^\dagger = \frac{1}{\sqrt{N}} \sum_{n=1}^N e^{inka} b_{qn}^\dagger, \quad (2.13)$$

and

$$u(q, k) = \sum_n e^{inka} u_n(q). \quad (2.14)$$

Then

$$\mathcal{H}_0 + \mathcal{H}_{\text{int}} = \sum_k \sum_{q>0} \hbar\omega(q, k) b_{qk}^\dagger b_{qk} \quad (2.15)$$

where the excitation frequencies are

$$\omega(q, k) = [v_F + u(q, k)]q. \quad (2.16)$$

The Coulomb interaction, regularised at short distances by a finite width w for edge states, has the form

$$U_n(x) = \frac{e^2}{4\pi\epsilon_0\epsilon_r} \frac{1}{\sqrt{x^2 + n^2a^2 + w^2}}. \quad (2.17)$$

The edge state width w is set by the localisation length ξ of localised states in the bulk of the sample at the Fermi energy. In a clean sample with well-separated Landau levels, $\xi \sim l_B$, but in a highly disordered sample with Landau levels that are broad in energy one may have $\xi \gg l_B$. The value of w proves important in matching our results to experiment, as we discuss in Sec. III D.

We write the Fourier transform, using the Poisson summation formula, as

$$u(q, k) = v_F \frac{\kappa}{2\pi} \sum_p \iint dx dz \frac{e^{-i(qx+kz+2\pi pz/a)}}{\sqrt{x^2 + z^2 + w^2}}. \quad (2.18)$$

and find

$$\omega(q, k) = v_F q \left(1 + \kappa \sum_{p \in \mathbb{Z}} Q_p^{-1} e^{-wQ_p} \right) \quad (2.19)$$

with $Q_p^2 = q^2 + (k + 2\pi p/a)^2$ and p integer. Here, the inverse screening length $\kappa \equiv e^2/4\pi\epsilon_r\epsilon_0\hbar v_F a$ characterises the interaction strength.

For isolated layers, taking the limit of large a , the sum on p may be replaced with an integral and one recovers the dispersion relation of edge magnetoplasmons in a single layer system, known from previous work.^{32,33}

For the multilayer system the expression for the dispersion relation may be simplified in two stages. First, if the layer spacing is small ($a \ll w$) the sum on p may be omitted, so that

$$\omega(q, k) = v_F q \left(1 + \frac{\kappa e^{-w\sqrt{q^2+k^2}}}{\sqrt{q^2+k^2}} \right). \quad (2.20)$$

If, in addition, interactions are weak ($w \ll \kappa^{-1}$)

$$\omega(q, k) = v_F q \left(1 + \frac{\kappa}{\sqrt{q^2+k^2}} \right). \quad (2.21)$$

In the following we obtain detailed results for systems with wide edges using the dispersion relation of Eq. (2.20), and for systems with narrow edges using the dispersion relation of Eq. (2.21).

D. Two-particle correlation function

A central quantity in our calculations of transport properties is the two-fermion correlation function

$$G(x, t) \equiv \langle \psi_n^\dagger(x, t) \psi_{n+1}(x, t) \psi_{n+1}^\dagger(0, 0) \psi_n(0, 0) \rangle, \quad (2.22)$$

where $\langle \dots \rangle \equiv \text{Tr}(e^{-\beta\mathcal{H}} \dots) / \text{Tr}(e^{-\beta\mathcal{H}})$ and operators are written in the Heisenberg representation, with $\mathcal{O}(t) = e^{i\mathcal{H}t/\hbar} \mathcal{O} e^{-i\mathcal{H}t/\hbar}$. We evaluate this in the absence of tunneling, so that $\mathcal{H} = \mathcal{H}_0 + \mathcal{H}_{\text{int}}$.

As a first step, define the boson field operator³⁴

$$\phi_n(x) = - \sum_{q>0} n_q^{-1/2} (e^{-iqx} b_{qn}^\dagger + e^{iqx} b_{qn}) e^{-\epsilon q/2} \quad (2.23)$$

where ϵ is a short-distance cut-off. Omitting Klein factors (which cancel from $G(x, t)$), the fermion and boson field operators are related by

$$\psi_n(x) = (2\pi\epsilon)^{-1/2} \exp(-i\phi_n(x)). \quad (2.24)$$

The correlation function is

$$G(x, t) = \frac{1}{(2\pi\epsilon)^2} \langle e^{i\phi_n(x, t)} e^{-i\phi_{n+1}(x, t)} e^{i\phi_{n+1}(0, 0)} e^{-i\phi_n(0, 0)} \rangle. \quad (2.25)$$

We define its logarithm S via

$$G(x, t) \equiv \frac{1}{(2\pi)^2} e^S. \quad (2.26)$$

Because \mathcal{H} is harmonic, S can be expressed as

$$\begin{aligned} S = & -\frac{1}{2} \langle (\phi_n(x, t) - \phi_{n+1}(x, t) + \phi_{n+1}(0, 0) - \phi_n(0, 0))^2 \rangle \\ & + \frac{1}{2} [\phi_n(x, t) - \phi_{n+1}(x, t), \phi_n(0, 0) - \phi_{n+1}(0, 0)] \\ & - 2 \log \epsilon. \end{aligned} \quad (2.27)$$

The thermal average and the commutator appearing in this expression can be evaluated in the standard way via a mode expansion, by expressing $\phi_n(x, t)$ in terms of boson creation and annihilation operators using Eq. (2.23). Taking the thermodynamic limit and so replacing wavevector sums with integrals, with $\beta = 1/k_B T$, we arrive at

$$S(x, t, T) = -2 \log \epsilon - \frac{a}{\pi} \int_{-\pi/a}^{\pi/a} dk (1 - \cos ak) \int_0^\infty \frac{dq}{q} e^{-\epsilon q} \\ \times \left(\coth(\beta \hbar \omega(q, k)/2) [1 - \cos(qx - \omega(q, k)t)] \right. \\ \left. + i \sin(qx - \omega(q, k)t) \right). \quad (2.28)$$

It is useful to note that

$$G(-x, -t) = G(x, t)^*, \quad (2.29)$$

and also to define a frequency-dependent correlator,

$$\tilde{G}(x, \Omega) = \int dt e^{i\Omega t} G(x, t). \quad (2.30)$$

III. CONDUCTIVITY

In this section we express the conductivity $\sigma(T)$ obtained from a Kubo formula in terms of the two-fermion correlation function calculated in Sec. II D. We also set out the steps required for a numerical evaluation of $\sigma(T)$, present our results, and compare them with the experimental data of Ref. 18.

A. Kubo formula for conductivity

The operator for the interlayer current density between layers n and $n + 1$ is

$$j_n(x) = \frac{ie}{\hbar} \left(t_\perp(n, x) \psi_{n+1}^\dagger(x) \psi_n(x) - \text{H. c.} \right). \quad (3.1)$$

The real part of the conductivity at frequency Ω is given by the Kubo formula³⁵

$$\sigma(\Omega, T) = \frac{ia}{\hbar \Omega L} \sum_m \int_{-\infty}^\infty dt \sin \Omega t \int dx \int dx' \\ \times \langle j_n(x, t) j_m(x', 0) \rangle. \quad (3.2)$$

To leading order, the interlayer hopping appears only in the current operators, and we evaluate the thermal average using a Hamiltonian from which interlayer hopping is omitted.

Substituting for $j_n(x, t)$ using Eq. (3.1) gives an expression for the conductivity of the chiral metal with a given

configuration of disorder: to leading order in $t_\perp(n, x)$,

$$\sigma(\Omega, T) = \frac{2iaL}{\hbar \Omega} \left(\frac{e}{\hbar L} \right)^2 \int dx \int dx' \int_{-\infty}^\infty dt \sin \Omega t \\ \times t_\perp(n, x) t_\perp^*(n, x') \\ \times \langle \psi_n^\dagger(x, t) \psi_{n+1}(x, t) \psi_{n+1}^\dagger(x', 0) \psi_n(x', 0) \rangle. \quad (3.3)$$

Averaging over disorder configurations yields

$$[t_\perp(n, x) t_\perp^*(n, x')]_{\text{av}} = t_\perp^2 e^{-|x|/l_{\text{el}}} \quad (3.4)$$

and hence

$$\sigma(\Omega, T) = \frac{e^2}{h} \frac{8\pi i a l_{\text{el}} t_\perp^2}{\Omega \hbar^2} \int \frac{dx}{2l_{\text{el}}} e^{-|x|/l_{\text{el}}} \int_{-\infty}^\infty dt \sin \Omega t \\ \times \langle \psi_n^\dagger(x, t) \psi_{n+1}(x, t) \psi_{n+1}^\dagger(0, 0) \psi_n(0, 0) \rangle. \quad (3.5)$$

This result can be expressed in terms of the time or frequency dependent two-particle correlation functions defined in Sec. II D. Setting $\Omega = 0$ we find

$$\sigma(T) = -\frac{e^2}{h} \frac{8\pi a l_{\text{el}} t_\perp^2}{\hbar^2} \int \frac{dx}{2l_{\text{el}}} e^{-|x|/l_{\text{el}}} \int_{-\infty}^\infty dt t \text{Im} G(x, t) \quad (3.6) \\ \equiv \frac{e^2}{h} \frac{8\pi a l_{\text{el}} t_\perp^2}{\hbar^2} \int \frac{dx}{2l_{\text{el}}} e^{-|x|/l_{\text{el}}} \text{Re} \left[\partial_\Omega \tilde{G}(x, \Omega) \Big|_{\Omega=0} \right].$$

For a boson dispersion relation $\omega(q, k) = v_F q$, as results from the Hartree approximation, the fermion correlation function factorises into independent contributions from each layer. These have the form

$$\langle \psi_n^\dagger(x, t) \psi_n(0, 0) \rangle = \frac{1}{2\pi} \int_{-\infty}^\infty dk \frac{e^{ik(v_F t - x)}}{1 + e^{\beta \hbar v_F k}} \quad (3.7)$$

and we find a temperature-independent conductivity

$$\sigma(\Omega, T) = \frac{e^2}{h} \frac{2t_\perp^2 l_{\text{el}} a}{\hbar^2 v_F^2} \frac{1}{1 + \Omega^2 l_{\text{el}}^2 / v_F^2}, \quad (3.8)$$

which in the zero-frequency limit has the value

$$\sigma_0 = \frac{e^2}{h} \frac{2t_\perp^2 l_{\text{el}} a}{\hbar^2 v_F^2}. \quad (3.9)$$

More generally, with an arbitrary boson dispersion relation a simplification of Eq. (3.6) is possible for $l_{\text{el}} \ll L_T$, since $G(x, t)$ varies with x only on the scale L_T while the correlator $[t_\perp(n, x) t_\perp^*(n, x')]_{\text{av}}$ has range l_{el} . We get

$$\sigma(T) = -4\pi \sigma_0 v_F^2 \int_{-\infty}^\infty dt t \text{Im} G(0, t) \\ \equiv 4\pi \sigma_0 v_F^2 \text{Re} \left[\partial_\Omega \tilde{G}(0, \Omega) \Big|_{\Omega=0} \right]. \quad (3.10)$$

B. Evaluation of $\sigma(T)$

To find the temperature dependence of the conductivity we must combine Eqs. (2.26), (2.28), and (3.10). A

first step before numerical evaluation is to isolate the dependence on the cut-off ϵ and take the limit $\epsilon \rightarrow 0$, as we describe in this subsection.

We start from the expression given in Eq. (2.28) for the logarithm of the two-particle correlation function, which we evaluate at $x = 0$. It is convenient to separate out a zero-temperature contribution by writing

$$S(t, T) \equiv S(t, 0) + \Delta S(t, T) \quad (3.11)$$

and also to split $S(t, 0)$ into real and imaginary parts, with

$$S(t, 0) \equiv \mathcal{U}(t) - i\mathcal{V}(t), \quad (3.12)$$

where $\mathcal{U}(t)$ and $\mathcal{V}(t)$ are real for t real. Then, writing

$$\sigma(T) = \sigma(0) + \Delta\sigma(T), \quad (3.13)$$

we obtain from Eq. (3.10)

$$\sigma(0) = \frac{2\sigma_0 v_F^2}{\pi} \int_0^\infty dt t e^{\mathcal{U}(t)} \sin \mathcal{V}(t) \quad (3.14)$$

and

$$\Delta\sigma(T) = \frac{2\sigma_0 v_F^2}{\pi} \int_0^\infty dt t e^{\mathcal{U}(t)} \sin \mathcal{V}(t) \left[e^{\Delta S(t, T)} - 1 \right]. \quad (3.15)$$

In the case of a linear boson dispersion relation, $\omega(q, k) = v_F q$, the functions $\mathcal{U}(t)$ and $\mathcal{V}(t)$ have the forms

$$\mathcal{U}_{\text{lin}}(t) = -\log(\epsilon^2 + v_F^2 t^2) \quad (3.16)$$

$$\mathcal{V}_{\text{lin}}(t) = \pi - 2 \tan^{-1}(\epsilon/v_F t). \quad (3.17)$$

Adding and subtracting these expressions from the ones for $\mathcal{U}(t)$ and $\mathcal{V}(t)$ with a general dispersion relation, we find

$$\begin{aligned} \mathcal{U}(t) &= \mathcal{U}_{\text{lin}}(t) + \frac{a}{\pi} \int_{-\pi/a}^{\pi/a} dk (1 - \cos ak) \\ &\times \int_0^\infty \frac{dq}{q} e^{-\epsilon q} [\cos(\omega(q, k)t) - \cos(v_F q t)] \end{aligned} \quad (3.18)$$

and

$$\begin{aligned} \mathcal{V}(t) &= \mathcal{V}_{\text{lin}}(t) + \frac{a}{\pi} \int_{-\pi/a}^{\pi/a} dk (1 - \cos ak) \\ &\times \int_0^\infty \frac{dq}{q} e^{-\epsilon q} [\sin(\omega(q, k)t) - \sin(v_F q t)]. \end{aligned} \quad (3.19)$$

Finally, we have

$$\begin{aligned} \Delta S(t, T) &= -\frac{a}{\pi} \int_{-\pi/a}^{\pi/a} dk (1 - \cos ak) \\ &\times \int_0^\infty \frac{dq}{q} e^{-\epsilon q} (1 - \cos \omega(q, k)t) \left[\coth\left(\frac{\beta \hbar \omega(q, k)}{2}\right) - 1 \right]. \end{aligned} \quad (3.20)$$

The advantage of casting the equations for the conductivity in this form is that the momentum integrals in

Eqs. (3.18), (3.19) and (3.20) can be performed at $\epsilon = 0$, since the integrands decay fast enough at large q for convergence. Dependence on ϵ is confined for small ϵ to the functions $\mathcal{U}_{\text{lin}}(t)$ and $\mathcal{V}_{\text{lin}}(t)$, and from Eqs. (3.16) and (3.17) one sees that it is important only for $t \sim \mathcal{O}(\epsilon)$. It is therefore convenient to separate the integration range in Eq. (3.14) into two parts, $0 \leq t < R$ and $R \leq t < \infty$, with $\epsilon \ll R \ll 1$. In the first interval $\mathcal{U}(t) = \mathcal{U}_{\text{lin}}(t)$ and $\mathcal{V} = \mathcal{V}_{\text{lin}}(t)$; in the second interval one can set $\epsilon = 0$.

Let the contributions to $\sigma(0)$ from the two intervals be $\sigma^{(1)}$ and $\sigma^{(2)}$. Writing $t' = v_F t/\epsilon$ we have

$$\sigma^{(1)} = \frac{2\epsilon^2 \sigma_0}{\pi} \int_0^{R\epsilon^{-1}} dt' t' e^{\mathcal{U}(t')} \sin \mathcal{V}(t') \quad (3.21)$$

which gives

$$\sigma^{(1)} = \frac{2\sigma_0}{\pi} \int_0^\infty dt' t' \frac{1}{1+t'^2} \frac{2t'}{1+t'^2} = \sigma_0. \quad (3.22)$$

Evaluation of $\sigma^{(2)}$ requires a numerical calculation, and we present results in Sec. III D.

Finally, turning to the conductivity at non-zero temperature, we note that there are no extra difficulties in the evaluation of $\Delta\sigma$ using Eq. (3.15). The function $\Delta S(t, T)$, can be computed numerically with $\epsilon = 0$, and $\Delta S(t, T) \rightarrow 0$ as $t \rightarrow 0$, so that $\Delta\sigma(T)$ has no contribution from the integration interval $0 \leq t < R$ in the limit $\epsilon \rightarrow 0$.

In summary, when evaluating $\sigma(0)$ or $\Delta\sigma(T)$ using Eqs. (3.14) and (3.15), the functions $\mathcal{U}(t)$, $\mathcal{V}(t)$, and $\Delta S(t, T)$ may be evaluated numerically by setting $\epsilon = 0$ in Eqs. (3.18), (3.19), and (3.20), and the results used in Eq. (3.14) to find $\sigma^{(2)}$. To this one must add $\sigma^{(1)} = \sigma_0$ in order to obtain the zero temperature conductivity $\sigma(0)$. These equations combine with Eq. (3.15) for $\Delta\sigma(T)$ to give a computationally tractable, though non-trivial, expression for $\sigma(T)$.

C. Conductivity at zero temperature

The conductivity at zero temperature and zero frequency is determined solely by the low energy limit of the group velocity for excitations, since no other modes are excited as $T, \Omega \rightarrow 0$. This zero frequency limit is reached as q , the wavevector component in the chiral direction, approaches zero. The group velocity, $\partial\omega(q, k)/\partial q|_{q=0} \equiv v_F \alpha(k)$, is in general a function of k , the wavevector component in the interlayer direction.

To determine $\sigma(0)$, a useful procedure is to consider a model dispersion relation which is exactly linear in q : $\omega(q, k) = v_F q \alpha(k)$. A linear dispersion relation is also of interest in its own right. It arises from an interaction that in real space is short range in the chiral direction, x : $U_n(x) = g_n \delta(x)$, giving $\alpha(k) = 1 + (2\pi \hbar v_F)^{-1} \sum_n e^{ikna} g_n$. With a linear dispersion relation, q -integrals in the expressions leading to $G(x, t)$ can be evaluated analytically, greatly simplifying the calculation

of conductivity. As we show in the following, for the limit $l_{\text{el}} \ll L_{\text{T}}$ that we consider, a dispersion relation linear in q yields a temperature-independent value of conductivity. For interactions, such as the Coulomb potential, that are not short range in x , linearisation of the dispersion relation gives only an approximation to $G(x, t)$. The value of $\sigma(0)$ that results from integrating this approximate form for $G(x, t)$ is nevertheless exact (at the leading order in t_{\perp} considered throughout this paper). This fact is clear on physical grounds, since we have correctly accounted for the dispersion relation at low energy. It may also be derived formally, as follows.

Starting from Eq. (3.10), we deform the contour for the time integral into the semicircle at infinity in the lower half of the complex plane, writing $t = t_R + it_I$ with t_R and t_I real. Then in Eq. (2.28) we have the factor

$$\int_0^{\infty} dq \frac{1}{q} \exp(-\epsilon q - iqx - it_R \omega(q, k) + t_I \omega(q, k)). \quad (3.23)$$

This must be evaluated for all values of t lying on the deformed time integration contour. When $|t_R|$ is large, $\exp(-it_R \omega(q, k))$ is a rapidly oscillating function of q , and the q -integral can be computed using the method of stationary phase: since $\omega(q, k)$ is a monotonically increasing function of q , the dominant contribution comes from the vicinity of the end-point at $q = 0$. Similarly, when t_I is large and negative, $\exp(t_I \omega(q, k))$ is small for most values of q , and the q -integral can be computed using steepest descents: again, the dominant contribution comes from the vicinity of $q = 0$. In both instances we may approximate $\omega(q, k)$ by its form linearised about $q = 0$; after linearisation the q -integral can be evaluated analytically.

This calculation yields

$$G(0, t) = \frac{1}{(2\pi)^2} \left(\frac{\pi t / \beta \hbar}{\sinh(\pi t / \beta \hbar)} \right)^2 \frac{1}{v_{\text{F}}^2} \frac{1}{(\epsilon + it)^2} \times \exp \left(-\frac{2a}{\pi} \int_0^{\pi/a} dk (1 - \cos ak) \log \alpha(k) \right). \quad (3.24)$$

Substituting this into Eq. (3.10) we obtain

$$\sigma(T) = \frac{2\sigma_0}{\pi} \exp \left(-\frac{2a}{\pi} \int_0^{\pi/a} dk (1 - \cos ak) \log \alpha(k) \right) \times \int \frac{dt \epsilon t^2}{(\epsilon^2 + t^2)^2} \left(\frac{\pi t / \beta \hbar}{\sinh(\pi t / \beta \hbar)} \right)^2. \quad (3.25)$$

In the limit $\epsilon \rightarrow 0$, the t integral gives $\pi/2$ regardless of temperature, demonstrating that, for systems with a linear dispersion relation, in the regime $l_{\text{el}} \ll L_{\text{T}}$, $\sigma(T)$ is independent of T . We find

$$\sigma(T) = \sigma_0 \exp \left(-\frac{2a}{\pi} \int_0^{\pi/a} dk (1 - \cos ak) \log \alpha(k) \right). \quad (3.26)$$

This is our final result for the dependence of $\sigma(0)$ on the dispersion relation as parameterised by $\alpha(k)$.

D. Results

We are now in a position to calculate the conductivity for a system with Coulomb interactions by evaluating numerically the formulae we have derived: first, the zero-temperature value using the results from Sec. III C, and then the full temperature-dependent conductivity using the results from Sec. III B. We investigate variation of the conductivity with two parameters, the Fermi velocity v_{F} and the edge state depth w , and seek values of these parameters for which our results match the experimental data of Ref. 18. The parameters enter the dispersion relation $\omega(q, k)$ directly, and v_{F} also appears in the inverse screening length κ . The interaction strength is set by the combination κa (recall that a is the layer spacing). A scale for temperature is set by v_{F} and a , via $T_0 \equiv \hbar v_{\text{F}} / a k_{\text{B}}$, so that $T/T_0 = a/L_{\text{T}}$. A scale for conductivity is given by σ_0 , its value in the Hartree approximation.

At a qualitative level, the effect of interactions on the conductivity can be anticipated by starting from the expression given in Eq. (3.9) for this quantity within the Hartree approximation. In turn, that expression can be understood in terms of a calculation of the interlayer tunneling rate, based on the Fermi golden rule: the rate involves the square of a matrix element between initial and final states on adjacent layers, and a power of the density of states for both the initial and the final states. The squared matrix element, allowing for disorder which affects phases of initial and final states separately, contributes a factor of $t_{\perp}^2 l_{\text{el}}$ to σ_0 . The form of the density of states on a single edge, $1/2\pi \hbar v_{\text{F}}$, implies that $\sigma_0 \propto v_{\text{F}}^{-2}$. Returning to a full treatment of the interacting system, we note that the effect of interactions is to generate an energy-dependent group velocity in place of a constant value, v_{F} . In effect, the value of $\sigma(T)$ at a particular temperature involves a thermal average of the inverse square of the group velocity. Because Coulomb interactions increase the group velocity at low energy, they decrease conductivity at low temperature; equally, because the group velocity approaches v_{F} at high energy, the conductivity approaches σ_0 at high temperature.

Turning to detailed results, the dependence of $\sigma(0)$ on w/a and κa is shown in Fig. 2, as obtained from Eq. (3.26) using $\alpha(k) = 1 + \kappa e^{-w|k|}/|k|$. Interactions reduce the value of the conductivity, by a factor which is large if κa is large. The variation of $\sigma(T)$ with T is illustrated in Fig. 3 for a system with the dispersion relation appropriate for narrow edge states, Eq. (2.21). In this case the k integrals in Eqs. (3.18) and (3.19) can be done analytically, leaving only the q and t integrals to be evaluated numerically. Finally, the behaviour of $\sigma(T)$ for a system with wide edge states ($w \geq a$) is presented in Fig. 4. In this case the dispersion relation is as given in Eq. (2.20), analytical progress does not seem possible, and integrals on k , q and t must be evaluated numerically to obtain $\sigma(T)$. We note in passing that we checked that there are only small changes to the results

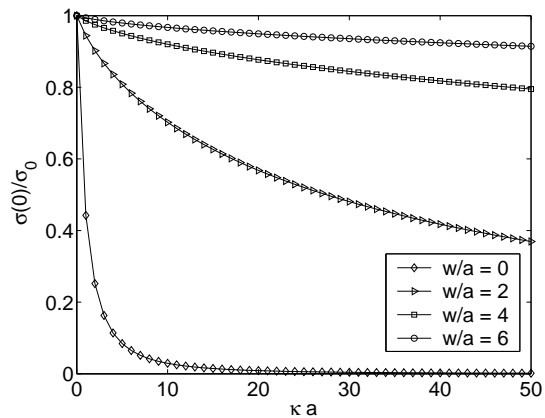


FIG. 2: Conductivity at zero temperature, as a function of interaction strength, parameterised by inverse screening length κ , for various edge state widths w .

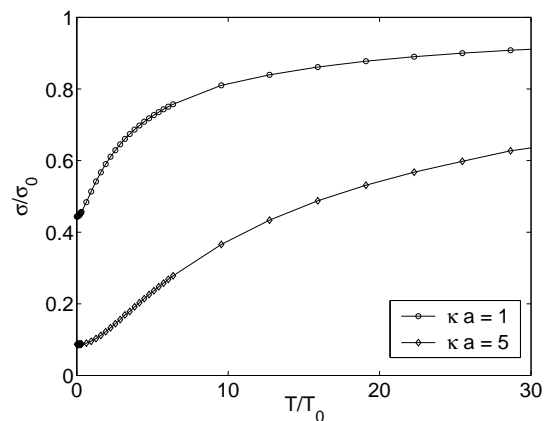


FIG. 3: Dependence of conductivity on temperature for narrow edge states, with interaction strengths $\kappa a = 1$ and $\kappa a = 5$.

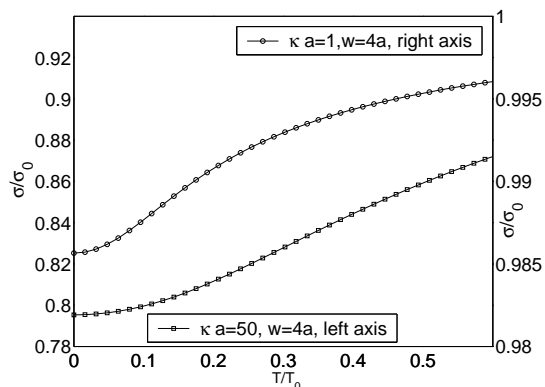


FIG. 4: Dependence of conductivity on temperature for wide edge states with $w = 4a$ and interaction strengths $\kappa a = 1$ and $\kappa a = 50$.

presented when using the more complete form of the interaction given in Eq. (2.19), including the sum on p .

Examining these results, it is evident that the general shape of $\sigma(T)$ does not vary greatly with parameters: the temperature dependence is quadratic at low temperatures, has a roughly linear region at intermediate temperatures, and approaches σ_0 in the high temperature limit. The quadratic dependence at low temperature is universal, but the extent of the roughly linear region at intermediate temperature is model-dependent. Moreover, scales in this temperature dependence change dramatically with parameter values. The value of the dimensionless temperature T/T_0 at the crossover between the low and intermediate temperature regimes is dependent on κ (see Fig. 3) and varies even more strongly with w (compare Figs. 3 and 4). In addition, the magnitude of the variation in $\sigma(T)$ between low and high T depends very much on the values of w and κa . In order to reproduce the experimental observation of a nearly linear increase in $\sigma(T)$, by about 7% between the temperatures of 50mK and 300mK,¹⁸ we require parameters which place the experimental temperature window in the intermediate regime for behaviour, so that quadratic variation of $\sigma(T)$ with T occurs only in a temperature range below 50 mK, and saturation of $\sigma(T)$ occurs only above 300mK. Since the available data is not sufficiently detailed to justify a formal fitting procedure, we instead survey the consequences of a range of parameter choices in our results and examine the match to experimental observations.

We begin by considering narrow edge states, using the results shown in Fig. 3. Supposing $v_F \sim \omega_{c/B}$, which represents an upper bound on v_F , we have $v_F = 1.7 \times 10^5 \text{ms}^{-1}$. With $a = 30\text{nm}$, we find $\kappa a \sim 1$ and $T_0 \sim 40\text{K}$. Taking these values, the variation in $\sigma(T)$ over the experimental temperature range is very small and quadratic, in disagreement with observations. A reduction in the value of v_F serves to decrease the temperature scale T_0 , and also increases κ . It is possible to generate approximately linear variation of $\sigma(T)$ with T in the experimental temperature range by using a sufficiently small value of v_F (reduced from the upper bound by $\sim \mathcal{O}(10^3)$), but we know of no reason for v_F to be so small.

We therefore turn to theoretical results for wide edge states, as illustrated in Fig. 4. In this case, we find that large values of w greatly reduce the temperature range over which $\sigma(T)$ varies quadratically with T , and can lead to approximately linear variation in the experimental temperature range. A second consequence of large w is that the conductivity change $\sigma(\infty) - \sigma(0)$ is reduced. This tendency can be counteracted by increasing the interaction strength κa . We find that observed behaviour can be reproduced by taking $w = 4a = 120\text{nm}$ and $v_F = 3 \times 10^3 \text{ms}^{-1}$ (giving $\kappa a = 50$). The temperature dependence of $\sigma(T)$ obtained using these parameter values is shown in Fig. 5 for temperatures below 400mK.

This choice of parameters, and its implications, merit

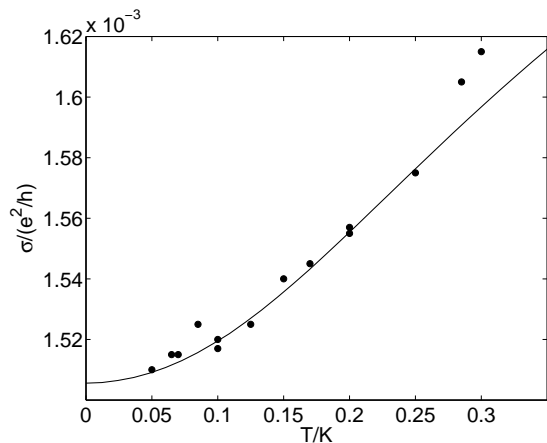


FIG. 5: Dependence of conductivity on temperature for $w = 4a$, with $a = 30\text{nm}$, $v_F = 3 \times 10^3\text{ms}^{-1}$ and $\sigma_0 = 1.893 \times 10^{-3}e^2/2\pi\hbar$ (full line), compared with experimental data (points) taken from Fig 2 of Ref. 18 (data set for Fractal 2).

further discussion. First, we note that there are two separate experimental indications that edge states have a width closer to the value we have adopted, of 120nm , than to the conventionally expected value of $l_B \simeq 10\text{nm}$. One comes from measurements of bulk hopping transport in multilayer samples³⁶, which give a localisation length of $\xi = 120\text{nm}$: one expects $w \simeq \xi$. The other comes from studies of conductance fluctuations,¹⁹ discussed in Sec. IV. These yield a value for the inelastic scattering length, from the amplitude of fluctuations, and a value for the area of a phase-coherent region perpendicular to the applied field, from the correlation field for fluctuations. The ratio of this phase-coherent area to the inelastic scattering length implies an edge state width which is also much larger than l_B : $w \simeq 70\text{nm}$. Next, turning to the value of v_F , which we have taken 50 times smaller than for edge states in a steep confining potential, we note that large edge state width favours a small value for v_F , because wide edge states penetrate into the bulk of the sample where both the confining potential gradient and the drift velocity of electrons moving in this potential are small. Finally, we comment on the fact that accepting a small value for v_F implies a large value for σ_0 , if other parameters are unchanged. In fact, large w acts in the opposite direction, to reduce the effective tunneling amplitude t_\perp between edge states, since different portions of the edge contribute to the amplitude with different phases, so that there are partial cancellations. To account for the magnitude of the measured¹⁸ conductivity, $1.5 \times 10^{-3}e^2/2\pi\hbar$, using the value for the mean free path $l_{el} = 30\text{nm}$ derived from magnetoresistance measurements¹⁷ requires an effective value of t_\perp about 50 times smaller than bare estimate³ of 0.12meV . This is a surprisingly strong suppression of tunneling, though possible if edge states in successive layers have different

displacements from the surface, as suggested in Ref. 18.

IV. CONDUCTANCE FLUCTUATIONS

It is found experimentally that mesoscopic fluctuations in the conductance of the chiral metal are induced by small changes of magnetic field within a quantum Hall plateau.^{12,19} These conductance fluctuations are observed in samples with a perimeter that is several times larger than the estimated inelastic scattering length. Under such conditions, it is not initially clear why the magnetic field component perpendicular to layers in the sample should influence conductance in this way, since in the simplest picture electron trajectories enclose flux only by encircling the sample. More realistically, a number of possibilities are evident:¹⁹ the sample walls may lie at an angle to the layer normal, either on average or because of surface roughness, or finite edge state width may be important. In our theoretical treatment of conductance fluctuations we avoid specific assumptions about this aspect of the system by considering fluctuations that result from variations in a magnetic field component B_\perp perpendicular to the sample surface. The amplitude of fluctuations is not affected by this choice. By contrast, the scale for the correlation field of fluctuations is dependent on the model chosen for flux linkage.

In a general setting, there are two possible reasons for the amplitude of conductance fluctuations to decrease with increasing temperature. One is because of a decrease in the inelastic scattering length; the other is because of thermal smearing. In the case of a chiral metal only the first mechanism operates, because states at different energies are perfectly correlated.⁹ In this sense, conductance fluctuations offer a rather direct probe of interaction effects.

In this section, in place of conductivity σ , we are concerned with the conductance $g = \sigma L/Na$ of a finite sample and fluctuations $\delta g = g - [g]_{av}$ about its average value. We denote the average within the Hartree approximation by $g_0 \equiv \sigma_0 L/Na$. We derive an analytic expression for the autocorrelation function of conductance fluctuations induced by B_\perp . We focus on its temperature dependence at low temperatures, obtaining a scaling form for the regime in which $\sigma(T) \approx \sigma(0)$. We compute the scaling function, evaluate our expressions numerically, and compare our results with the observations of Ref. 19.

A. Correlation function

The conductance autocorrelation function

$$F(\delta B) = [\delta g(B_\perp)\delta g(B_\perp + \delta B)]_{av} \quad (4.1)$$

is characterised by the amplitude $F(0)$ and by the correlation field. An obvious field scale is set by a flux density of one flux quantum Φ_0 through a rectangle with sides

proportional to the layer spacing and the thermal length, and we define $B_0 = \Phi_0/2\pi aL_T = \hbar/eaL_T$. We also introduce a dimensionless field variation $b = \delta B/B_0$, which depends on temperature through L_T , and a temperature-independent reduced field h which has dimensions of wavevector: $h = b/L_T \equiv e\delta B/a\hbar$.

With a suitable choice of gauge, the transverse field enters the Hamiltonian only as a phase for interlayer hopping. Taking for convenience $B_\perp = 0$, in the presence of non-zero δB Eq. (2.9) is modified to

$$t_\perp(n, x) = t_\perp e^{i(\theta_{n+1}(x) - \theta_n(x) + hx)}. \quad (4.2)$$

This additional, field-dependent phase alters \mathcal{H}_{hop} and consequently the current operator.

An expression for the conductance of a sample with a specific disorder configuration is obtained by scaling Eq. (3.3) with the sample dimensions. Taking account of the field-dependent phases in the current operator and substituting into the definition of $F(\delta B)$, after some manipulation we arrive at

$$\begin{aligned} F(\delta B) &= \frac{g_0^2 \pi^2 v_F^4}{L^2 l_{\text{el}}^2 N^2} \sum_{n,m} \int dx \int dx' \int dy \int dy' \quad (4.3) \\ &\times \int dt it G(x - x', t) \int dt' it' G(y - y', t') \\ &\times \left(e^{ih(x-x')} + e^{-ih(x-x')} \right) e^{C(x,x')} e^{C(y,y')} \\ &\times \left(e^{D_{nm}(x,x'; y,y')} + e^{-D_{nm}(x,x'; y,y')} - 2 \right). \end{aligned}$$

Two contributions to this expression arise from the disorder average:

$$C(x, x') = -\frac{1}{2} [(\theta_{n+1}(x) - \theta_n(x) - \theta_{n+1}(x') + \theta_n(x'))^2]_{\text{av}} \quad (4.4)$$

and

$$\begin{aligned} D_{nm}(x, x'; y, y') &= [(\theta_{n+1}(x) - \theta_n(x) - \theta_{n+1}(x') + \theta_n(x')) \\ &\times (\theta_{m+1}(y) - \theta_m(y) - \theta_{m+1}(y') + \theta_m(y'))]_{\text{av}}. \quad (4.5) \end{aligned}$$

Both may be evaluated using the result (for $x, y > 0$)

$$[\theta_n(x)\theta_m(y)]_{\text{av}} = \frac{\delta_{nm}}{l_{\text{el}}} \min\{x, y\}. \quad (4.6)$$

The equation for C gives

$$e^{C(x,x')} = e^{-|x-x'|/l_{\text{el}}}, \quad (4.7)$$

which in the limit of small l_{el} can be written $2l_{\text{el}}\delta(x-x')$. The expression for D is more complicated: one finds

$$D_{nm}(x, x'; y, y') = \frac{R(x, x'; y, y')}{l_{\text{el}}} (2\delta_{nm} - \delta_{n+1, m} - \delta_{n-1, m}). \quad (4.8)$$

The function $R(x, x'; y, y')$ gives the overlap between the two directed intervals on the real line $x \rightarrow x'$ and $y \rightarrow$

y' : for example, $R(1, 5; 4, 9) = -R(5, 1; 4, 9) = 1$. On substituting these expressions for C and D into Eq.(4.3), we obtain

$$\begin{aligned} F(b) &= \frac{g_0^2 \pi^2 v_F^4}{L^2 l_{\text{el}}^2 N^2} \int dx \int dx' \int dy \int dy' (e^{ih(x-x')} + e^{-ih(x-x')}) \\ &\times \int dt it G(x - x', t) \int dt' it' G(y - y', t') e^{-|x-x'|/l_{\text{el}}} \\ &\times e^{-|y-y'|/l_{\text{el}}} \left\{ e^{2R(x,x'; y,y')/l_{\text{el}}} + e^{-2R(x,x'; y,y')/l_{\text{el}}} - 2 \right. \\ &\left. + 2e^{R(x,x'; y,y')/l_{\text{el}}} + 2e^{-R(x,x'; y,y')/l_{\text{el}}} - 4 \right\}. \quad (4.9) \end{aligned}$$

Examining where the weight of the integrand lies with respect to the spatial integrals in Eq. (4.9), one sees that the term in braces vanishes except in places where $R \neq 0$. We consider different types of contributions from these regions, and keep only those which are leading order for $L_T \gg l_{\text{el}}$. First, consider regions in which $|x-y| \sim l_{\text{el}}$ but $|x-x'| \gg l_{\text{el}}$. The small factor $e^{-|x-x'|/l_{\text{el}}}$ is compensated by the first term in the braces if $|x' - y'| \sim l_{\text{el}}$. Then

$$e^{-|x-x'|/l_{\text{el}}} e^{-|y-y'|/l_{\text{el}}} e^{2R(x,x'; y,y')/l_{\text{el}}} = e^{(-|x-y| - |x'-y'|)/l_{\text{el}}}. \quad (4.10)$$

Since $G(x, t)$ has a range in x of order L_T , the resulting contribution to $F(\delta B)$ is $\mathcal{O}(L_T/L)$. Another contribution of the same order arises from regions where $|x - y'| \sim l_{\text{el}}$ and $|x' - y| \sim l_{\text{el}}$. Subleading contributions come from regions where all four spatial variables are within an elastic length of one another. These contributions are $\mathcal{O}(l_{\text{el}}/L)$.

Keeping only the leading order terms, the expression for the correlation function has the much simplified form

$$\begin{aligned} F(\delta B) &= \frac{4g_0^2 \pi^2 v_F^4}{NL} \int dx (e^{ihx} + e^{-ihx}) \int dt it \int dt' it' \\ &\times (G(x, t)G(x, t') + G(x, t)G(-x, t')). \quad (4.11) \end{aligned}$$

Using the symmetry of $G(x, t)$ (see Eq. (2.29)) one finds

$$F(\delta B) = \frac{g_0^2}{NL} \int_{-\infty}^{\infty} dx e^{ihx} [f(x)]^2, \quad (4.12)$$

where

$$f(x) \equiv -4\pi v_F^2 \int_{-\infty}^{\infty} dt t \text{Im}G(x, t). \quad (4.13)$$

B. Computing the correlation function

In order to compare our theory for conductance fluctuations with experiment, we need to be able to calculate $F(\delta B)$ for various values of the temperature and parameters v_F and w . Although it is possible to use a computer to evaluate the form of $F(B_\perp)$ given in Eq. (4.12) without further approximation, it is far easier to make progress

by calculating $G(x, t)$ for a linearised dispersion relation. This approach is exact in the low-temperature regime defined by the condition $\sigma(T) \approx \sigma(0)$, and we proceed to use it in our calculations.

In the low temperature regime where the linearised dispersion relation may be used, $F(B_\perp)$ has a scaling form. To make this apparent, it is helpful to recast equations in terms of dimensionless variables, characterising δB by b in place of h , and introducing $\hat{x} = x/L_T$ and $\hat{t} = v_F t/L_T$. Writing $G(x, t) = (2\pi L_T)^{-2} \hat{G}(\hat{x}, \hat{t})$ and $f(L_T \hat{x}) = \hat{f}(\hat{x})$, for a linear dispersion relation, $\omega(q, k) = qv_F \alpha(k)$, we have

$$\begin{aligned} \hat{G}(\hat{x}, \hat{t}) &= \exp \left\{ \frac{-2a}{\pi} \int_0^{\pi/a} dk (1 - \cos ak) \right. \\ &\times \left[\log |\hat{x} - \alpha(k)\hat{t}| - \log \left(\frac{\pi[\alpha(k)\hat{t} - \hat{x}]/\alpha(k)}{\sinh(\pi[\alpha(k)\hat{t} - \hat{x}]/\alpha(k))} \right) \right] \left. \right\} \\ &\times \exp \left\{ -ia \int_0^{\pi/a} dk (1 - \cos ak) \operatorname{sgn}(\hat{x} - \alpha(k)\hat{t}) \right\} \quad (4.14) \end{aligned}$$

and

$$\hat{f}(\hat{x}) = -\frac{1}{\pi} \int_{-\infty}^{\infty} dt \hat{t} \operatorname{Im} \{ \hat{G}(\hat{x}, \hat{t}) \}. \quad (4.15)$$

Then the conductance autocorrelation function has the form

$$F(\delta B) = \frac{g_0^2 L_T}{NL} C(\delta B/B_0) \quad (4.16)$$

with scaling function

$$C(b) = \int_{-\infty}^{\infty} d\hat{x} e^{ib\hat{x}} [\hat{f}(\hat{x})]^2. \quad (4.17)$$

In this form $F(\delta B)$ depends on temperature T and magnetic field difference δB only through the scaling variables L_T/L and $\delta B/B_0$. The thermal length L_T plays the role of an inelastic scattering length, in the sense that it determines both the amplitude of conductance fluctuations and (through B_0) their correlation field. Such behaviour is initially surprising, since L_T is independent of interaction strength. In fact, of course, the form of the scaling function $C(b)$ depends parametrically on interaction strength.

For weak interactions this dependence of $C(b)$ on κ can be extracted analytically, as follows. First, note from Eq. (2.21) that $\alpha(k) = 1 + \kappa/|k|$. Also, in Eqs. (4.14), (4.15) and (4.17), change variables from \hat{x}, \hat{t} to y, p with $\hat{x} = y/\kappa$ and $\hat{t} = yp + y/\kappa$. Then

$$\begin{aligned} \lim_{\kappa \rightarrow 0} \hat{G}(y/\kappa, yp + y/\kappa) &\equiv g(y, p) \\ &= \exp \left\{ \frac{-2a}{\pi} \int_0^{\pi/a} dk (1 - \cos ak) \right. \\ &\times \left[\log |y(p + 1/k)| - \log \left(\frac{\pi y[p + 1/k]}{\sinh(\pi y[p + 1/k])} \right) \right] \left. \right\} \\ &\times \exp \left\{ ia \int_0^{\pi/a} dk (1 - \cos ak) \operatorname{sgn}(y[p + 1/k]) \right\} \end{aligned}$$

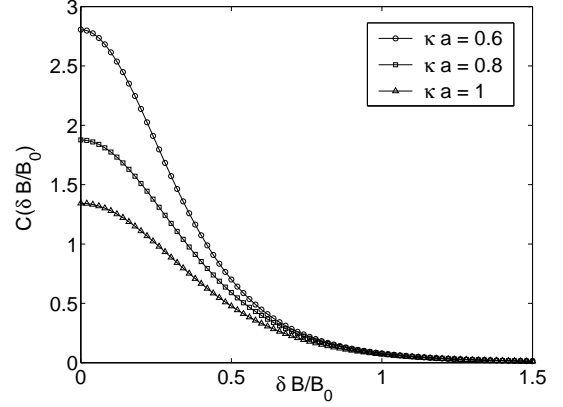


FIG. 6: $C(\delta B/B_0)$ for narrow edge states and $\kappa a = 0.6, 0.8$, and 1.

and

$$\lim_{\kappa \rightarrow 0} \hat{f}(y/\kappa) \equiv \tilde{f}(y) = -\frac{y^2}{\pi} \int_{-\infty}^{\infty} dp p \operatorname{Im} \{ g(y, p) \}.$$

The κ -dependence of the scaling function is hence isolated for small κ as

$$C(b) = \frac{1}{\kappa} \int_{-\infty}^{\infty} dy \exp(iyb/\kappa) [\tilde{f}(y)]^2, \quad (4.18)$$

demonstrating that the amplitude of conductance fluctuations grows and that the correlation field shrinks as interactions are made weaker. In both cases, the variation implies an inelastic scattering length that diverges as κ^{-1} for weak interactions. Such a dependence of the inelastic scattering length on interaction strength is long-established in non-chiral, one-dimensional conductors.³⁷

In order to find the form of the scaling function and to study its κ -dependence at general κ , a three-dimensional numerical integration is necessary. We compute $\hat{G}(\hat{x}, \hat{t})$, then $\hat{f}(\hat{x})$, and then the scaling function $C(b)$ itself.

C. Results

We illustrate the form of the scaling function $C(\delta B/B_0)$ for a range of parameter values in a sequence of three figures. Its dependence on interaction strength κa is shown for narrow edge states in Fig. 6 and for $w = a$ in Fig. 7. In both cases, smaller interaction strength leads to a larger amplitude for conductance fluctuations and a smaller correlation field, as may be anticipated on the grounds that weaker interactions lead to a longer inelastic scattering length. In Fig. 8 $C(\delta B/B_0)$ is shown for $\kappa = 50$ and $w = 4a$, the parameter values suggested by the comparison of our conductivity calculations with experiment. We discuss experimental data on conductance fluctuations in Sec. IV D. Finally, the increase in the amplitude of conductance fluctuations with decreasing κ is illustrated in Fig. 9.

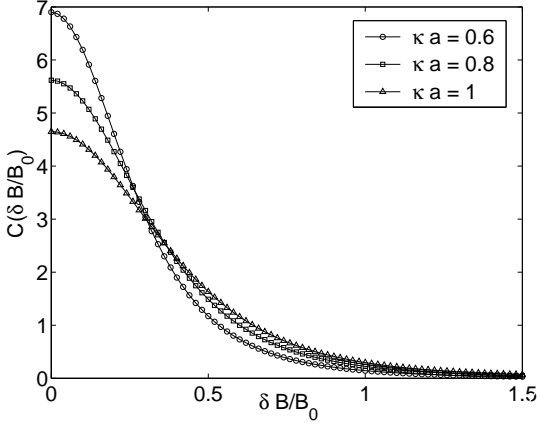


FIG. 7: $C(\delta B/B_0)$ for $w = a$ and $\kappa a = 0.6, 0.8,$ and $1.$

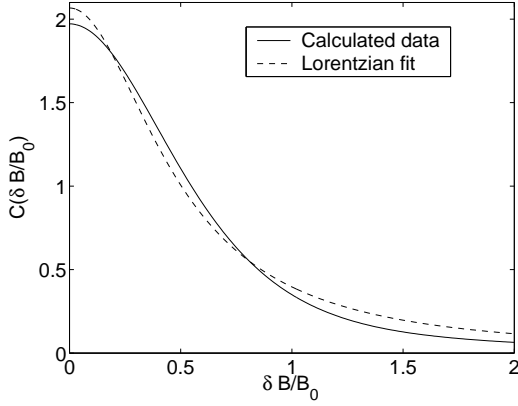


FIG. 8: $C(\delta B/B_0)$ at $w = 4a$ and $\kappa a = 50.$

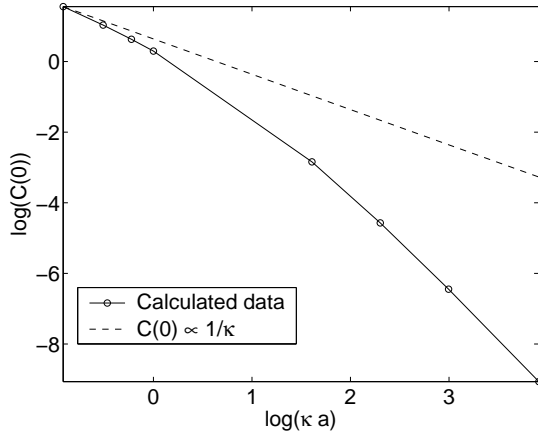


FIG. 9: Conductance fluctuation amplitude as a function of interaction strength κa at $w = 0$ (full line), and asymptotic behaviour calculated analytically for small κa (dashed line)

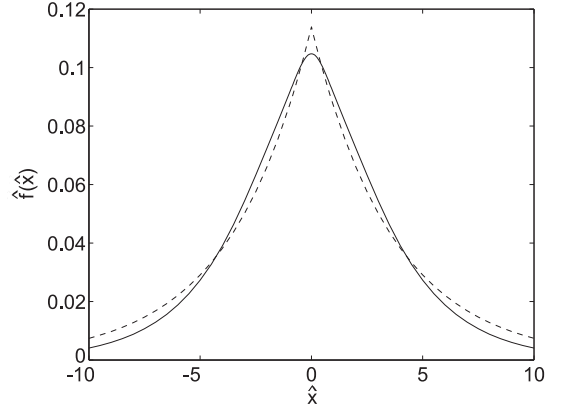


FIG. 10: $\hat{f}(\hat{x})$ calculated at $\kappa a = 50$ and $w = 4a$ (solid line) compared with the best fitting exponential decay (dashed line).

D. Comparison with experiment and previous theory

The exact treatment of disorder and interactions provided by the calculations we have described presents an opportunity to test the standard theoretical treatment of conductance fluctuations, in which a single inelastic scattering length l_{in} , or equivalently a scattering rate $v_{\text{F}}/l_{\text{in}}$ is used as a cut-off in perturbation theory. For the chiral metal, such calculations have been described in Ref. 9. They yield a Lorentzian scaling function

$$F(\delta B) = \frac{2g_0^2}{NL} \frac{l_{\text{in}}}{1+z^2} \quad (4.19)$$

with $z = 2\pi\delta B l_{\text{in}} a / \Phi_0$. A comparison between the functional form we obtain for $F(\delta B)$ and a Lorentzian is given in Fig. 8: while the two functions are similar, the discrepancies are worth attention because they indicate behaviour which cannot be characterised by a single relaxation time. A similar comparison can be made in the Fourier transformed domain, in terms of the function $f(x)$. To reproduce Eq. (4.19) from our Eq. (4.12), we would require $l_{\text{in}} = L_{\text{T}}$ and

$$\hat{f}(\hat{x}) = e^{-|\hat{x}|/2}, \quad (4.20)$$

where exponential decay is indicative of a single lifetime $l_{\text{in}}/v_{\text{F}}$ for excitations. The form we obtain for $\hat{f}(\hat{x})$ is shown in Fig. 10. The absence of a cusp at $x = 0$ indicates that there is of a range of relaxation times in the system. In addition, the fact that $f(0) \neq 1$ is an interaction effect (from Eq. (3.10) one sees that $f(0) = \sigma(0)/\sigma_0$) not allowed for in the standard perturbative treatment.

We close this section with a comparison between the experiments of Ref. 19 and our results, using the same parameters, $\kappa a = 50$ and $w = 4a$, that provided a match for the behaviour of $\sigma(T)$. For the experimental base temperature of $T = 70\text{mK}$, we use our approach to determine the amplitude of conductance fluctuations. As

a way to present the result, we then follow the experimental analysis¹⁹ in using Eq. (4.19) to obtain a value for l_{in} of $0.3\mu\text{m}$. The experimental value, extracted in the same way, is $l_{\text{in}} \sim 1\mu\text{m}$. Since the calculated amplitude of conductance fluctuations varies by several orders of magnitude over the range of parameter values we have investigated, and since no new adjustment of parameters was involved in our discussion of conductance fluctuations, we find the rough agreement between these two values of l_{in} very encouraging.

V. CONCLUSIONS

In summary, for the system of weakly coupled quantum Hall edge states that we have studied, bosonisation provides a very complete treatment of the interplay between electron-electron interactions and disorder. We have shown that interaction effects can account for the observed temperature dependence of interlayer conductivity, provided we allow for finite edge state width and

adopt a value for the edge state velocity that is rather smaller than previously supposed. We have investigated conductance fluctuations within the same theoretical approach, showing how they are suppressed with increasing temperature, with a characteristic lengthscale $L_T \propto T^{-1}$. Encouragingly, the same parameter values used to match the measured behaviour of conductivity reproduce approximately the observed fluctuation amplitude. From a theoretical viewpoint, it is interesting that such dephasing effects can be generated from a description based on harmonic collective modes, simply via the nonlinear relation between boson and fermion operators.

Acknowledgments

We thank E. G. Gwinn for very helpful discussions and J. J. Betouras for previous collaborations. The work was supported by EPSRC under Grant GR/R83712/01 and by the Dutch FOM foundation.

-
- ¹ J. T. Chalker and A. Dohmen, Phys. Rev. Lett. **75**, 4496 (1995).
² L. Balents and M. P. A. Fisher, Phys. Rev. Lett. **76**, 2782 (1996).
³ D. P. Druist, P. J. Turley, K. D. Maranowski, E. G. Gwinn, and A. C. Gossard, Phys. Rev. Lett. **80**, 365 (1998).
⁴ H. Mathur, Phys. Rev. Lett. **78**, 2429 (1997).
⁵ I. A. Gruzberg, N. Read, and S. Sachdev, Phys. Rev. B **55**, 10593 (1997).
⁶ S. Cho, L. Balents, and M. P. A. Fisher, Phys. Rev. B **56**, 15814 (1997).
⁷ V. Plerou and Z. Q. Wang, Phys. Rev. B **58**, 1967 (1998).
⁸ J. T. Chalker and S. L. Sondhi, Phys. Rev. B **59**, 4999 (1999).
⁹ J. J. Betouras and J. T. Chalker, Phys. Rev. B **62**, 10931 (2000).
¹⁰ D. P. Druist, P. J. Turley, E. G. Gwinn, K. D. Maranowski, and A. C. Gossard, Physica B **249**, 70 (1998).
¹¹ B. Zhang *et al.*, Physica B **256**, 279 (1998).
¹² D. P. Druist *et al.*, Superlattices and Microstructures **25**, 181 (1999).
¹³ M. Kuraguchi and T. Osada, Physica E **6**, 594 (2000).
¹⁴ D. P. Druist, E. G. Gwinn, K. D. Maranowski, and A. C. Gossard, Physica E **6**, 619 (2000).
¹⁵ D. P. Druist, E. G. Gwinn, K. D. Maranowski, and A. C. Gossard, Physica E **12**, 129 (2002).
¹⁶ H. A. Walling *et al.*, Physica E **12**, 132 (2002).
¹⁷ D. P. Druist, E. G. Gwinn, K. D. Maranowski, and A. C. Gossard, Phys. Rev. B **68**, 075305 (2003).
¹⁸ H. A. Walling *et al.*, Phys. Rev. B **70**, 045312 (2004).
¹⁹ H. A. Walling, E. G. Gwinn, K. D. Maranowski, J. Xu, and A. C. Gossard, Phys. Rev. B **70**, 235343 (2004).
²⁰ J. W. Tomlinson, J.-S. Caux, and J. T. Chalker, Phys. Rev. Lett. **94**, 086804 (2005).
²¹ X. G. Wen, Phys. Rev. B **41**, 12838 (1990).
²² X. G. Wen, Phys. Rev. Lett. **64**, 2206 (1990).
²³ X. G. Wen, Phys. Rev. B **43**, 11025 (1990).
²⁴ A. M. Chang, Rev. Mod. Phys. **74**, 1449 (2003).
²⁵ J. D. Naud, L. P. Pryadko, and S. L. Sondhi, Phys. Rev. Lett. **85**, 5408 (2000).
²⁶ J. D. Naud, L. P. Pryadko, and S. L. Sondhi, Nucl. Phys. B **594**, 713 (2001).
²⁷ K. Moon and S. M. Girvin, Phys. Rev. B **54**, 4448 (1996).
²⁸ U. Zülicke and A. H. MacDonald, Phys. Rev. B **54**, R8349 (1996).
²⁹ Y. Oreg and A. Finkel'stein, Phys. Rev. B **54**, R14265 (1996).
³⁰ L. P. Pryadko, E. Shimshoni, and A. Auerbach, Phys. Rev. B **61**, 10929 (2000).
³¹ J. von Delft and H. Schoeller, Annalen Phys. **7**, 225 (1998).
³² V. A. Volkov and S. A. Mikhailov, JETP Lett. **42**, 556 (1985).
³³ V. A. Volkov and S. A. Mikhailov, Sov. Phys. JETP **67**, 1639 (1988).
³⁴ Eqns. (2.23) and (2.28) correct sign errors in Eqns. (8) and (13) of Ref. 20. None of the results of Ref. 20 are changed by these corrections.
³⁵ This version of the Kubo formula does not distinguish between the external, applied field and an internal, screened field. The distinction is unimportant in our context because screening in the chiral metal of an electric field in the interlayer direction vanishes in the long wavelength limit.⁹ See Ref. 29 for a related discussion. One of us (J. T. C.) is grateful to D. G. Polyakov for a discussion of this point.
³⁶ H. A. Walling, E. G. Gwinn, K. D. Maranowski, and A. C. Gossard, Phys. Rev. B **71**, 045327 (2005).
³⁷ W. Apel and T. M. Rice, J. Phys. C **16**, L271 (1983).